Characterization of Second-Life Lithium-Ion Batteries from a Solar-Powered Electric Bus for Stationary Applications

Matheus Hohmann[1], Aline K. V. de Oliveira[1], Lucas A. Z. Sergio[1], Daniel O. dos Santos[1], Leonardo F. Pacheco[12], Ricardo Rüther[1] and Helena F. Naspolini[1]

[1] FOTOVOLTAICA/UFSC Laboratory, Florianópolis (Brazil)

[2] CELESC - Power Plants of Santa Catarina, Florianópolis (Brazil)

Abstract

This work presents the electrical and thermal characterization of second life lithium-ion battery modules from the solar electric bus (eBus) of the Federal University of Santa Catarina (UFSC), with the aim of assessing their feasibility for applications in transportable storage systems within the CELESC and UFSC project. In total, 149 modules were analyzed under controlled charge and discharge tests to determine state of health (SoH), direct current internal resistance (DCIR), and the electrical characteristic curves of these battery modules. The results indicated a strong negative correlation between SoH and DCIR $R^2 = 0.80$, validating DCIR as an effective parameter for estimating the level of degradation and the remaining capacity of the batteries. Modules that remained in continuous operation in the e-Bus exhibited greater degradation SoH between 58% and 64%, whereas the reserve modules maintained better conditions SoH between 66% and 69%. The results confirm the technical potential for repurposing these batteries in stationary energy storage systems, provided they undergo appropriate requalification and balancing processes. The study contributes to advancing the circular economy applied to electric mobility and to the development of standardized methodologies for evaluating second life batteries.

Keywords: Second-life lithium-ion batteries; Battery repurposing; State of Health (SoH); Direct current internal resistance (DCIR); Electric Bus; Transportable battery energy storage systems.

1. Introduction

The global energy transition has driven the advancement of electric mobility as one of the strategic pillars for decarbonizing the transport sector. Regulatory incentives, technological evolution, and new consumption models have promoted the accelerated expansion of the global electric fleet. According to recent data from the International Energy Agency (2025), global sales of electric vehicles surpassed 17 million units in 2024, representing growth of more than 20% compared with the previous year. In parallel, climate policies, such as the European regulation that requires all new urban buses to be zero emission by 2035, reinforce the role of electrified public transport as a vector of urban sustainability.

This scenario, however, brings new challenges related to the life cycle of traction batteries. After reaching approximately 80% of their nominal capacity, these batteries no longer meet the autonomy and performance requirements demanded for vehicular use, yet they still retain suitable conditions for reapplication in stationary energy storage systems (Ruan et al., 2023; S et al., 2024). This concept, known as second life of batteries, has attracted growing research and investment interest, especially because it combines environmental benefits, by extending the useful life of materials and reducing the demand for new cells, with economic advantages for distributed generation systems and smart grids.

In the Brazilian context, the e-Bus project of the Federal University of Santa Catarina (UFSC) played a pioneering role in introducing electric mobility solutions integrated with photovoltaic generation. Initiated in 2016 and operated for six years with solar energy supplied by the Fotovoltaica UFSC Laboratory (https://fotovoltaica.ufsc.br/sistemas/fotov/en/ 3 minutes video on the eBus available), the vehicle traveled more than 135 thousand kilometers transporting students and researchers between the central campus and Sapiens Park in Florianopolis (Antoniolli, 2017; Oliveira et al., 2019). The battery pack supplied by Mitsubishi

10.18086/swc.2025.06.07 Available at http://proceedings.ises.org

Heavy Industries underwent gradual degradation until its complete replacement with a new lithium iron phosphate LFP set, creating an opportunity for the reuse and analysis of the decommissioned batteries.

The batteries removed from the e-Bus were incorporated into a research and development project carried out jointly by CELESC (Centrais Elétricas de Santa Catarina S.A.) and the UFSC. The project, developed under the Brazilian Electricity Regulatory Agency's (ANEEL) R&D Program, aims to design and implement transportable energy storage systems using both first-life and second-life lithium-ion batteries applied to the electrical distribution grid. Among its objectives are the assessment of the reuse potential and operational safety of second-life batteries through standardized protocols for electrical, thermal, and safety characterization. Such procedures enable the determination of key parameters, including State of Health (SoH) and Direct Current Internal Resistance (DCIR), as well as the establishment of technical criteria for the requalification and reintegration of these batteries into new stationary applications.

Following their retirement from the e-Bus, the Li-ion batteries underwent rigorous characterization testing, as detailed in this study, to verify their performance and confirm their suitability for stationary applications. The characterized batteries will ultimately be integrated into a Transportable Battery Energy Storage System (TBESS, or "battery-on-wheels"), designed to support electrical distribution networks. Mounted on a semi-trailer, the TBESS combines first-life and second-life batteries, achieving a total storage capacity of 400 kWh and a power output of 150 kW. This innovative storage solution provides strategic advantages for managing seasonal peak demand, ensuring reliability during scheduled or emergency outages, and supporting grid stability by regulating voltage and reactive power. Its modular and transportable configuration allows flexible deployment in high-demand locations, significantly enhancing grid resilience and operational flexibility.

Several recent studies have demonstrated the relevance of fast and reliable techniques for the evaluation of second life batteries, including tests based on multivariate pulses, surface thermal monitoring, and adaptive SoH estimators (Cui et al., 2025; Hong et al., 2025; Tao et al., 2025). The correlation between internal resistance and capacity, already observed in automotive batteries of different origins (Hohmann et al., 2024), reinforces the potential of such metrics as effective indicators of electrochemical aging. In parallel, standards such as UL 1974 and IEC 62660 1 have provided guidelines for the safe reuse of modules, covering processes from individual screening to the reassembly of packs with homogeneous characteristics.

Despite the progress achieved, the standardization and practical application of characterization methodologies at industrial scale still pose challenges. Differences in usage history, non-uniform degradation, and lack of traceability hinder comparative evaluation between batches and applications. Thus, the present study proposes and applies an experimental procedure for electrical and thermal characterization of second life modules from the e-Bus from UFSC, with the purpose of assessing their performance, identifying predominant degradation mechanisms, and establishing reference parameters for the future use of these batteries in transportable storage systems for application in distribution systems.

2. Methodology

The methodology employed in the characterization of second life battery modules from the e-Bus was developed to preserve the physical integrity of the components analyzed and to ensure the reliability of the results obtained. In total, 149 modules were examined, of which two numbers 155 and 156, although manufactured in the same lot as the others, were never used in the electric vehicle and therefore remained in unused condition.

The other 147 modules were arranged in banks composed of 11 modules connected in series, all effectively used during bus operation. It is worth noting that not all banks operated simultaneously. There was a rotation system among the sets, in which eight banks remained in use on the e-Bus while the others were reserved for replacements or periodic maintenance.

All banks were removed from the e-Bus, duly opened and disconnected, to allow the individual extraction of the modules for subsequent characterization. The battery module analyzed in this study consists of eight P140 cells connected in series (Figure 1), with a nominal voltage of 29.6 V at 50% State of Charge (SOC) and 25

°C and a nominal capacity of 50 Ah. These parameters result in a total energy of approximately 1.48 kWh, with a volumetric energy density of 121 Wh/L and a gravimetric energy density of 98 Wh/kg. Each cell has a nominal voltage of 3.7 V, operating in the range from 2.7 V to 4.2 V, and a nominal capacity of 50 Ah equivalent to 185 Wh. The maximum continuous charge and discharge current is 100 A, reaching peaks of up to 300 A for periods of up to 10 s.

```
Model                          : Eight P140 cells connected in series
Nominal Voltage                : 29.6 V (@SOC = 50 %, 25 °C)
Voltage Range                  : 21.6 – 33.6 V
Nominal Capacity               : 50 Ah (5hr @ 25 °C)
kWh Capacity                   : 1.48 kWh
Operational Humidity           : 20 – 90 % RH
Operating Temperature Range
     Discharge                 : -20 – +50 °C
     Charge                    : 0 – 50 °C
Module Dimension               : W 379mm, D 140mm, H 230mm
Weight                         : 15 kg
```

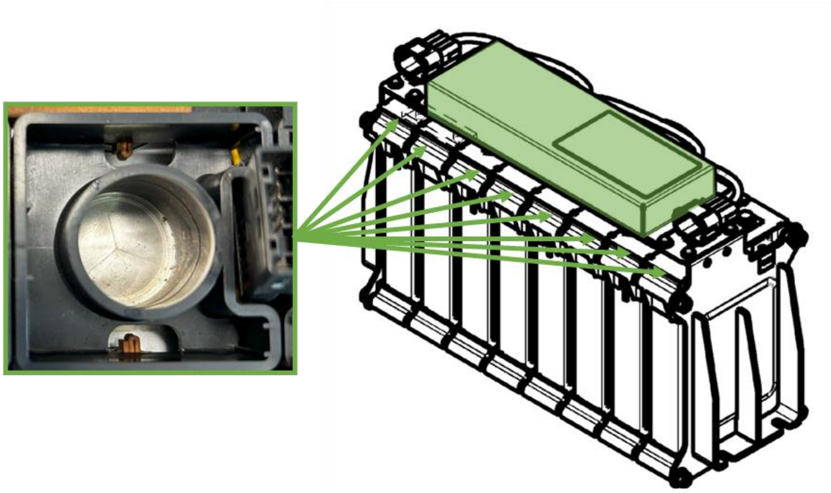

Figure 1: Specifications and 3D model of the evaluated second life module, composed of eight P140 cells in series 29.6 V; 50 Ah; 1.48 kWh. The original BMS is highlighted by the orange box, and the arrows indicate the positions of the safety valves of each cell.

3.1 Teste Bench

To characterize the cells, a test bench (Figure 2) was assembled, composed of equipment specific to each stage of the experimental process. A RIGOL electronic load, model DL3031, was employed for discharge control, with an operating range of up to 150 V, a maximum current of 60 A, and a power limit of 350 W. This equipment enabled the programming of discharge profiles and data acquisition at the module level, with current and voltage measurements performed with an accuracy of 0.001 A and 0.001 V, respectively.

The battery charging process was conducted using an ITECH IT6722A power supply, capable of delivering up to 80 V, 20 A, and 400 W. Like the electronic load, the power supply had a serial communication interface, allowing remote configuration of charging parameters and data reading at the module level. Both devices were fundamental to ensure the accuracy and reliability of the results obtained in the characterization tests of the lithium-ion batteries.

Given that the power supply and the electronic load did not have resources for the individual reading of cell voltage, a dedicated acquisition system was developed using an ESP32 microcontroller associated with ADS1115 analog digital converters. This system enabled individual monitoring of the eight cells of the module, in addition to the integration of five PT100 sensors for temperature measurement and a controller circuit intended for the actuation of the power contactors from the original battery system of the Nissan LEAF.

Complementarily, a Python language code was developed for configuration, control, and safety supervision during the characterization tests. The program was also responsible for acquiring the data measured by monitoring devices and for the automatic storage of the information in files in .csv format, intended for the subsequent processing and analysis of the results.

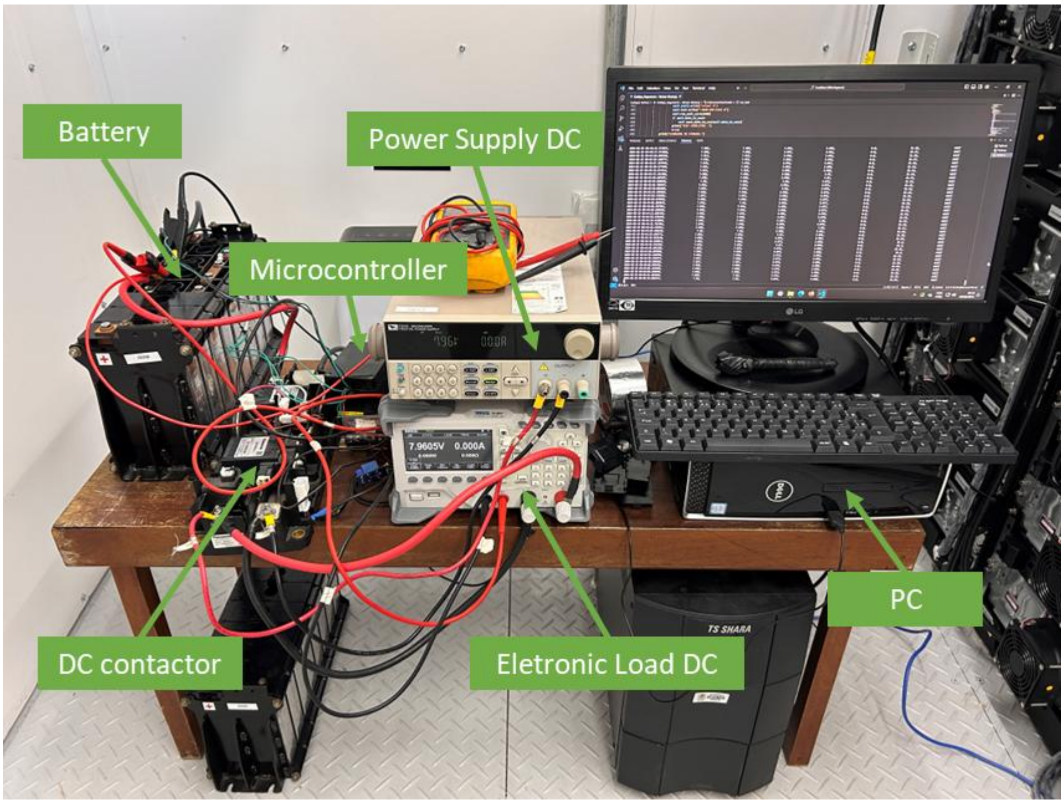

Figure 2: Test bench for electrical characterization of second life modules, composed of an electronic load Rigol DL3031, a programmable power supply ITECH IT6722A, an ESP32 ADS1115 acquisition system, and PT100 sensors.

3.2 Characterization Tests

The characterization of batteries, whether first-life or second-life, is a fundamental step for evaluating their electrochemical performance. In this phase, charge and discharge tests are carried out to determine operating curves and essential electrical parameters, such as SoH and DCIR. In both cases, the characterization methodology follows similar experimental principles and is based on equivalent mathematical models, which enables comparisons and extrapolations between new and used batteries (Azizighalehsari et al., 2024; Gharebaghi et al., 2025).

In the case of first-life cells, performing complete characterization tests is not a recurring practice, since manufacturer standardization and quality control ensure batch uniformity. In such contexts, testing is often limited to verifying basic parameters, such as voltage and DCIR, using specific equipment (Salek et al., 2024). A widely used metric to evaluate first-life storage systems is the Round-Trip Efficiency (RTE) (eq. 1) (Beckers et al., 2023), which expresses the ratio between the energy released during a complete discharge and the energy required for the subsequent recharge:

$$RTE\ (\%) = \left(\frac{E_{Discharge}}{E_{Charge}}\right) \times 100 \qquad \text{(eq. 1)}$$

On the other hand, the characterization of second life batteries requires particular attention to the determination of SoH and DCIR, which are critical parameters for evaluating the condition and current performance of the battery. The remaining capacity, obtained by comparing the current capacity with the first life nominal capacity, is the main indicator of the feasibility of reusing the cells in new applications. In parallel, DCIR, by reflecting internal losses and the energy efficiency of the system, is directly associated with thermal behavior and the rate of degradation over time. A deep understanding of these parameters provides support for determining the suitability of second life batteries in different application contexts, contributing to the efficient use of energy resources (Adebanjo et al., 2025; Akram & Abdul-Kader, 2024; Azizighalehsari et al., 2024).

The characterization process was structured in controlled charge and discharge stages. In the method proposed in this study, the module was initially connected to the test bench and subjected to a constant current charge of C/5 until reaching 33.6 V equivalent to 4.2 V per cell, in accordance with the voltage limit specified by the manufacturer. The end of the charge was identified when the current reached the cutoff value of C/50 or when one of the cells reached 4.22 V. In such cases, charging was stopped preventively for safety reasons, without interrupting the test. After charging, the module remained at rest for 10 minutes before the start of the discharge.

After the complete charging of the module, discharges were carried out with a current of C/5 in a pulsed profile, alternating discharge and rest periods of 10 minutes each (Böttiger et al., 2017). The discharge was conducted until one of the cells reached 2.8 V. Thereafter, the modules were recharged with a constant current of C/5 for 60 minutes, avoiding storage at low SOC levels (Adebanjo et al., 2025).

Throughout all characterization procedures, individual monitoring of cell voltage was performed, in addition to temperature measurement for each pair of cells, with an additional sensor dedicated to monitoring ambient temperature. The tests were conducted in a controlled environment, with temperature and humidity maintained at 20 °C and 60% RH. Before the start of the tests, the batteries remained in thermal equilibrium with the environment for a minimum period of 12 hours after their entry into the test bench environment.

The determination of capacity and SoH was performed during the discharge stage of the module, based on the integration of current as a function of time eq. 2, resulting in the measured capacity, expressed in ampere hour Ah. The SoH value was obtained by normalizing the measured capacity with respect to the first-life nominal capacity (eq. 3):

$$Measured\ Capacity\ (Ah) \ = \int i(t)\ dt \qquad \text{(eq. 2)}$$

$$SoH\ (\%) = \frac{Measured\ Capacity}{First\ Life\ Capacity} * 100 \qquad \text{(eq. 3)}$$

The calculation of DCIR was carried out exclusively during the pulsed discharge test, making use of the transition between rest and discharge periods. To determine this parameter, the difference between the open circuit voltage (V_{oc}) and the voltage when connected to a load (V_t), associated with the average discharge current (I_{med}), was used, as expressed in eq. 4. The measurements of voltage under load were taken 20 seconds after the start of the discharge:

$$DCIR(m\Omega) = \frac{V_{oc} - V_t}{I_{med}} * 1000 \qquad \text{(eq. 4)}$$

3.3 Data Analysis

All data processing and graph generation were performed using the Python programming language, with emphasis on the use of the pandas and matplotlib libraries. The data acquisition rate was configured at 4 Hz, to ensure safety and control during the stages of the characterization test. However, for the calculation of parameters such as capacity and DCIR, such a high sampling frequency was not necessary. Thus, all raw files obtained during the tests were resampled to a temporal base of 1 second, using the mean of the values within each interval.

In the data processing script, routines were implemented for the calculation of capacity and DCIR of each tested module. For the capacity calculation, a filter was applied to the main data frame to identify the periods corresponding to battery discharges. From the current values and the time records, discrete integration of the data was carried out to determine the effective capacity and, consequently, the SoH associated with the module.

In the calculation of DCIR, the instants in which the test status transitioned from "wait" to "discharge" were identified, corresponding to the start of each current pulse. For each of these pulses, the open circuit voltage Voc was defined as the value measured two seconds before the start of the discharge, while the voltage under load V_t was obtained 20 seconds after the start of the pulse, and the corresponding current value Imed was also recorded. With these parameters, eq. 4 was applied for each cell, obtaining the individual DC resistance for each pulse.

Repeating this procedure for all pulses allowed the construction of the DCIR curve along the discharge. Finally, the total resistance of the module was determined by the sum of the individual resistances of the cells at each pulse, providing a complete overview of the evolution of internal resistance during the discharge process.

3. Results

This section presents the results obtained from the characterization tests carried out with the second life modules, followed by the respective data analysis. During the evaluation process, it was verified that some modules exhibited anomalous behaviors, not fully meeting the criteria defined in the proposed methodology. As a result, they were excluded from the final analysis.

In total, 19 modules were disregarded: 003, 008, 020, 021, 029, 030, 047, 050, 054, 055, 065, 073, 075, 076, 084, 095, 117, 128, and 155. It is emphasized that this exclusion does not imply the technical infeasibility of the modules, but only the absence of suitable experimental conditions to ensure comparability and consistency of the results obtained.

Figure 3 presents the characteristic discharge curves of the analyzed modules, illustrating the relationship between total module voltage and the corresponding SOC. Each curve is individually identified by the module number, while the color scale on the right correlates the modules with their respective SoH values, ranging from 55 % indicating greater degradation (purple) to 95 % representing lower degradation (yellow).

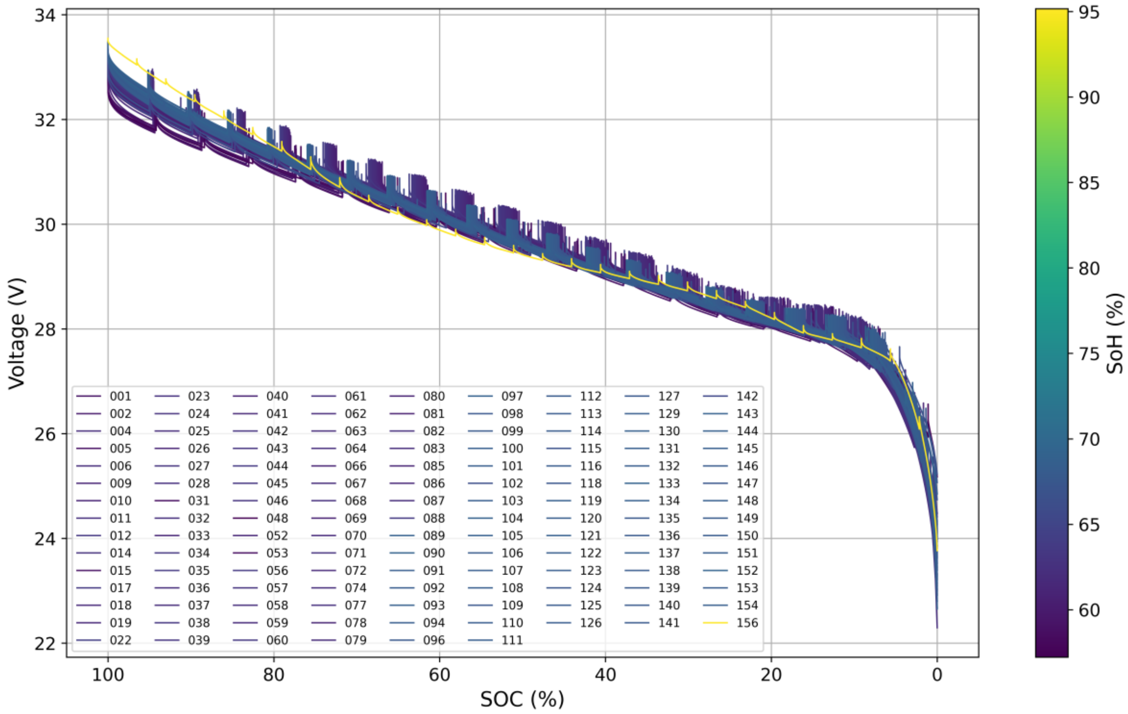

Figure 3: Discharge curves V × SOC of the evaluated modules. The coloring indicates the SoH of each module, ranging from 55% (purple) to 95% (yellow). A marked drop in voltage is observed below 20% SOC.

The analysis of the graph reveals that, although there is slight dispersion among the curves, all modules exhibit very similar overall behavior. A gradual decline in average voltage is observed as SOC decreases to approximately 20 %, from which point the drop becomes more pronounced, a behavior typical of lithium-ion batteries. This characteristic reflects the electrochemical phenomenon inherent to the discharge process, in which the variation of potential occurs in a nonlinear manner as the active material is reduced.

Another relevant aspect evidenced in Figure 3 concerns the influence of SoH on the discharge curve. It is noted that modules with lower SoH represented by purple tones exhibit lower voltages throughout the entire process compared with those with higher SoH in green and yellow tones. Nevertheless, the general shape of the curves remains practically unchanged, indicating that degradation affects above all the usable capacity and energy autonomy, without significantly modifying the electrochemical dynamics of the discharge process. In practical terms, this result demonstrates that even in the most degraded modules the discharge behavior remains consistent, which reinforces the feasibility of reuse of these components in stationary applications or in systems that employ conventional converters, provided they are properly characterized and classified according to their state of health.

Figure 4 presents the relationship between DCIR and module voltage, with each point on the graph corresponding to an individual DCIR measurement at a given voltage value. A clear dependence is observed between these parameters. In states near full charge voltages around 33.6 V, DCIR values are higher and show greater dispersion, reflecting greater heterogeneity among the cells under this condition. As the voltage decreases to the intermediate range between 28.8 and 30.4 V, the resistance values stabilize at a lower level between approximately 25 and 45 mΩ, indicating an ideal operating region, characterized by lower thermal dissipation and higher energy efficiency. When voltages reach the deep discharge region below 27.2 V, there is again a marked increase in resistance and variability among the cells, a behavior associated with the loss of ionic conductivity and the depletion of active materials in the electrodes.

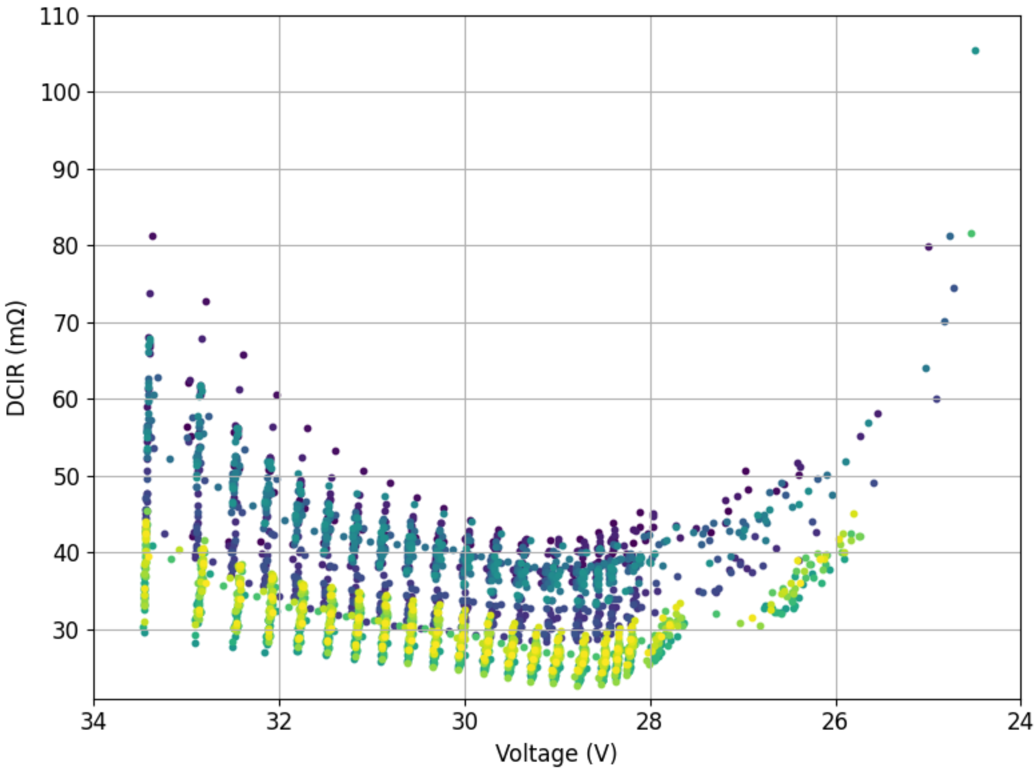

Figure 4: Direct current internal resistance (DCIR) as a function of module voltage. Higher values and dispersion are noted at high states of charge greater than 32 V and low less than 28 V, with stability in the intermediate range 28.8 to 30.4 V.

From the joint analysis of the V × SOC and DCIR × V curves, it is verified that both the available capacity and the internal resistance undergo systematic variations throughout the discharge cycle. These results provide the basis for investigating in an integrated manner the relationship between SoH and DCIR, since the increase in internal resistance can serve as an indirect indicator of the level of degradation of the modules. This correlation is illustrated in Figure 5, which presents the results obtained during the characterization test of module 129, including three main curves that represent the physical parameters associated with the electrochemical performance of the battery. The graph also indicates a SoH value of 68.11% for the analyzed module.

The upper curve shows the variation of the average cell voltage as a function of SOC during the constant current discharge test C/5. A gradual and almost linear drop in voltage is noted, ranging from approximately 4.05 V to around 3.4 V, which characterizes a stable discharge regime for most of the test. Near the end, a sharp drop in voltage is observed, typical of the depletion of usable capacity in lithium-ion batteries.

The intermediate curve represents the variation of the average DCIR of the module per cell, obtained from the tests with pulsed current at different SOC levels. A characteristic U-shaped behavior is observed, in which the internal resistance is higher at the extremes SOC near 100% and 0% and minimal in the intermediate region. This pattern arises from the increase in resistances associated with electrochemical phenomena at the electrode interfaces, especially at extreme states of charge, where there is greater polarization and limitations in ion diffusion.

Finally, the lower curve illustrates the variations in the average module temperature and ambient temperature throughout the constant current discharge test. A progressive rise in the average module temperature is observed, from approximately 20 °C at the beginning to 23.5 °C at the end of the test, a trend consistent with the heat generation resulting from internal resistive losses. The ambient temperature maintained small oscillations around 20 °C, attributed to climate control in the laboratory during the tests.

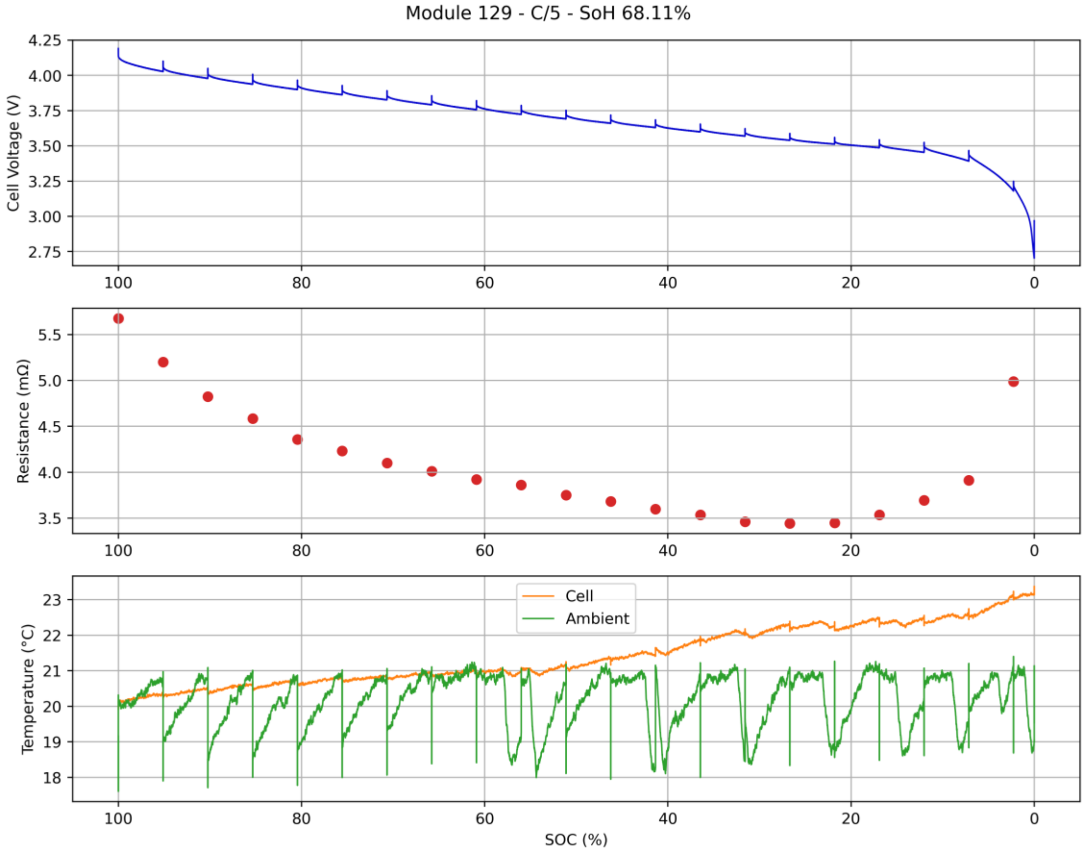

Figure 5: Results of the tests of module 129: voltage × SOC curve under constant discharge C/5 (upper); variation of DCIR as a function of SOC (intermediate); evolution of module temperature and ambient temperature (lower).

Figure 6 presents the distribution of SoH and DCIR values of the tested cells, organized according to the pack of origin. The analysis of SoH reveals the presence of two distinct groups. While packs numbered from 1 to 8 display lower average values, predominantly between 58 % and 64 %, packs 9 to 14 concentrate higher values, mostly between 66 % and 69 %.

This difference is directly related to the operation of the e-Bus battery system, in which only eight packs were used simultaneously, while the other six remained as a backup. Consequently, packs 1 to 8 were subjected to a considerably higher number of charge and discharge cycles, resulting in more pronounced degradation. Packs 9 to 14, used less intensively, exhibited reduced wear, consistent with the shorter effective time of use.

The DCIR results reinforce this distinction between the active packs and the backup packs. Cells from packs 1 to 8 present notably higher internal resistance values, with several observations between 35 and 45 mΩ, indicating an advanced process of electrochemical degradation. In contrast, packs 9 to 14 exhibit significantly lower DCIR values, concentrated below 30 mΩ, which suggests better preservation of the active materials and reduced thickening of the electrode electrolyte interface layer Solid Electrolyte Interphase – SEI.

However, the behavior of packs 3 and 4 stands out, as they present DCIR values like those of packs 9 to 14, yet with substantially lower SoH. This discrepancy indicates the action of degradation mechanisms predominantly related to capacity loss, without proportional variation of internal resistance. Such phenomena may be associated with the irreversible loss of lithium available for ionic exchange Loss of Lithium Inventory – LLI or with the structural fragmentation of the active electrode materials, processes that reduce storage capacity without significantly compromising internal electrical conductivity.

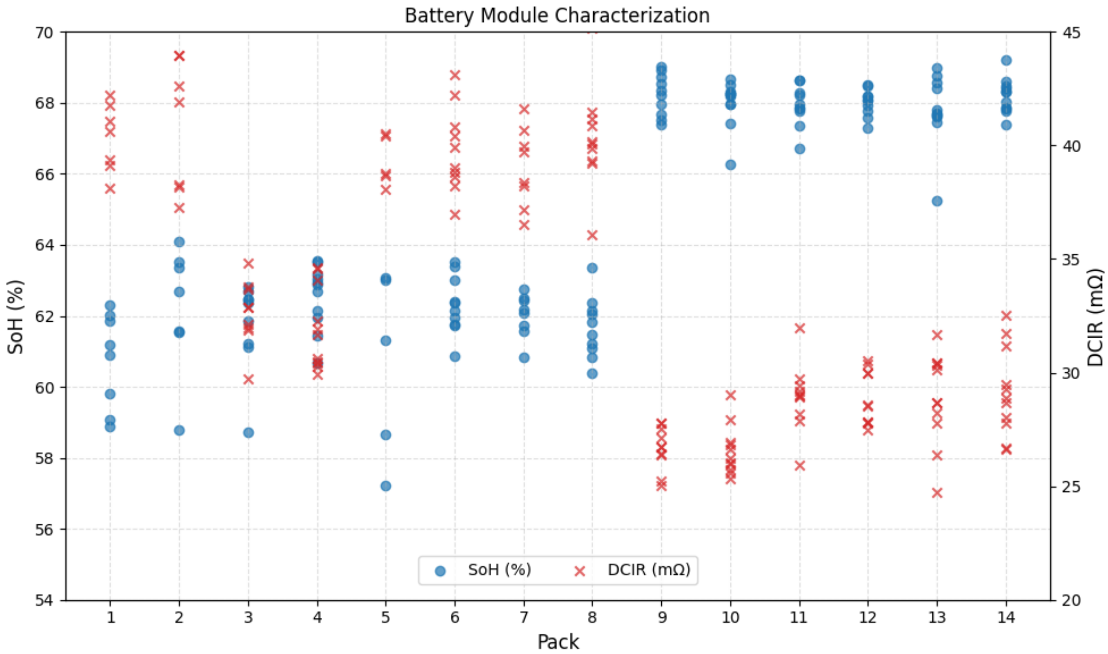

Figure 6: SoH and DCIR results for second life Li ion battery modules relative to their respective original pack.

The analysis of the spatial variation of DCIR as a function of the physical position of the cells within the packs did not reveal systematic correlations indicating location associated degradation. Although local thermal variations may occur, no consistent patterns were observed linking specific positions to higher resistance values. These results suggest that the observed degradation arises mainly from global operational factors, such as time of use, average depth of discharge, and average operating temperature, rather than internal structural aspects of the pack arrangement.

It is worth noting that the e-Bus battery bank was equipped with an active cooling system, composed of fans responsible for exhausting hot air in the battery compartment. The absence of significant variations among cell positions, together with the homogeneous thermal behavior observed, indicates that the ventilation system efficiently performed its function under the operational conditions analyzed. This finding reinforces the importance of adequate thermal management mechanisms, since batteries operating without active ventilation tend to present greater thermal heterogeneity and accelerated degradation (Hohmann et al., 2024).

Figure 7 presents the relationship between SoH, in %, and DCIR, in mΩ, for the different second life battery packs evaluated, identified by their respective IDs according to the color scale. This analysis aimed to investigate the existence of a correlation between the increase in internal resistance and the degradation of the usable capacity of the modules. Each point on the graph represents the average SoH and DCIR values corresponding to a given pack.

The results show a well-defined negative trend between SoH and DCIR, as demonstrated by the linear regression represented by the red line. The coefficient of determination $R^2 = 0.80$ indicates that approximately 80 % of the variation in state of health can be explained by the variation in internal resistance, suggesting that this is a reliable indicator of the level of electrochemical degradation of the modules analyzed.

It is observed that packs with resistance below 30 mΩ are concentrated mostly in the SoH range between 67 % and 69 %, whereas those with resistance above 38 mΩ tend to present SoH below 63 %. This behavior reinforces the hypothesis that the increase in internal resistance is associated with electrode aging, growth of passivating layers, such as the Solid Electrolyte Interphase (SEI), and other structural and electrochemical changes that negatively affect the usable capacity of the modules.

However, significant dispersion is noted in the intermediate resistance intervals between 30 and 38 mΩ, in which modules with intermediate DCIR values are observed but with SoH varying between 61 % and 63 %. This variability can be explained by the action of distinct and independent degradation mechanisms that affect capacity and internal resistance of the cells in different ways.

For example, increases in resistance may occur due to thickening of the SEI layer, degradation of current collectors, or deterioration of internal contacts, without necessarily implying significant loss of cyclable lithium or active material, resulting in similar capacities but with different DCIR values. Conversely, reductions in capacity may be associated with the loss of lithium available for ionic exchange Loss of Lithium Inventory LLI or with fragmentation of the electrode particles, which limits storage capacity without causing expressive increases in internal resistance (Edge et al., 2021; Liu et al., 2014; O'Kane et al., 2022).

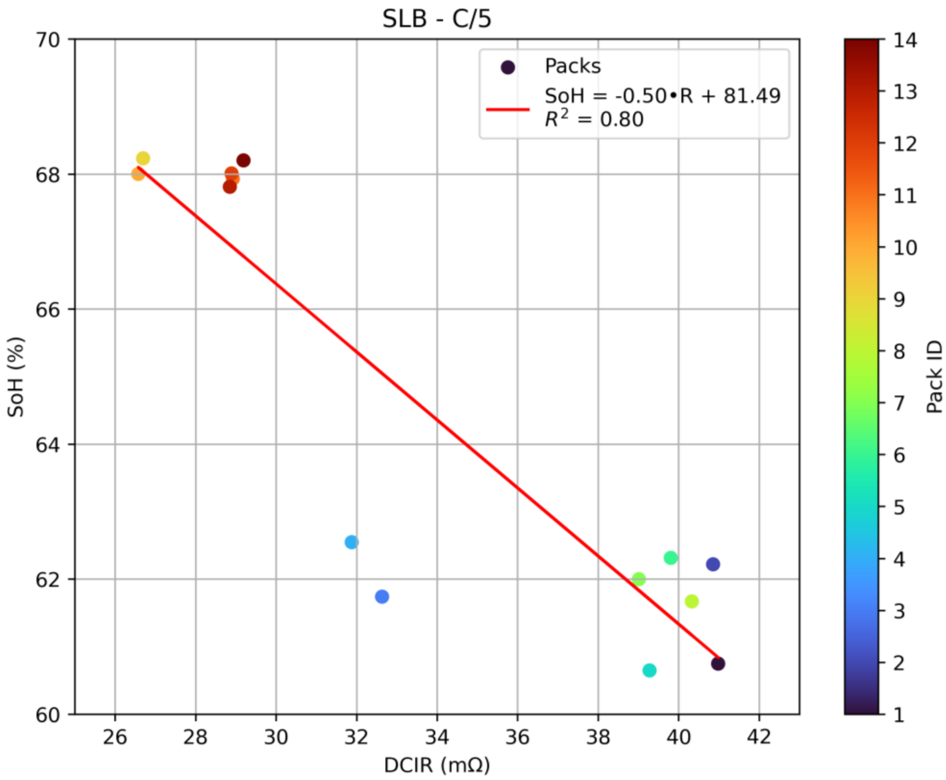

Figure 7: Relationship between SoH % and average DCIR mΩ of the tested packs. The linear regression red line shows a negative correlation R² = 0.80.

Thus, the dispersion observed in the relationship between SoH and DCIR shows that different aging and degradation trajectories act heterogeneously on the electrical parameters of the modules, even under similar operational conditions. This result reinforces the need for multivariate approaches in the evaluation of battery aging, simultaneously considering electrochemical, thermal, and structural aspects for a more comprehensive understanding of the behavior of second life cells.

4. Conclusion

This study presented a comprehensive experimental characterization of second life lithium-ion battery modules originally employed in the solar electric bus of UFSC e-Bus and later reintegrated into the CELESC UFSC R&D project on transportable storage systems with first life and second life batteries. The methodology employed, based on pulsed current discharge, proved effective for identifying different aging profiles among the modules. The results revealed that approximately 80 % of the variation in SoH can be explained by the variation in DCIR, confirming a good correlation $R^2 = 0.80$ between these parameters. This correlation validates DCIR as a rapid diagnostic indicator to estimate the residual capacity and overall condition of repurposed lithium-ion batteries.

Two main degradation patterns were observed. Packs that remained in more intensive operation in the e-Bus system exhibited lower SoH values 58 % to 64 % and higher DCIR levels 35 to 45 mΩ, whereas those that operated less frequently showed better preservation, with SoH between 66 % and 69 % and DCIR below 30 mΩ. These results demonstrate the clear influence of usage intensity on the electrochemical aging process. Even so, the more degraded modules still presented stable and predictable discharge behavior, maintaining profiles suitable for stationary systems of low to medium power.

From an applied point of view, the characterized modules show good performance for reintegration into stationary systems for distributed generation, peak demand control, or backup applications. The operating range identified between 28.8 V and 30.4 V represents an ideal region of efficiency and thermal stability, which can guide the design of converters and management strategies for second life storage systems.

The experimental procedure proposed in this study provides a reproducible and scalable methodology for evaluating second-life vehicle batteries under Brazilian conditions. Beyond the technical validation of reuse, it establishes quantitative parameters that support decision-making in industrial requalification processes, as well as regulatory standardization and safety assurance. Furthermore, the correlation between SoH and DCIR obtained in this work offers valuable input for the development of predictive algorithms in battery management systems (BMS), enabling real-time monitoring and adaptive operation of second-life modules.

Future work may expand this framework through automation and the integration of analysis tools based on data, eventually incorporating artificial intelligence techniques for automatic classification of degradation patterns and lifetime prediction. In addition, extending the characterization protocol to include prolonged cycling tests, impedance spectroscopy, and simulations of thermal runaway will enhance the understanding of the behavior of these batteries in different operational scenarios.

In summary, this study reinforces the technical feasibility and environmental relevance of repurposing traction batteries in stationary applications. By quantifying the relationship between electrochemical health indicators and operational performance, it contributes to a circular economy model in which electric mobility and renewable energy systems converge toward more sustainable and efficient storage solutions.

5. Acknowledgments

The authors express their sincere gratitude to the Brazilian Electricity Regulatory Agency (ANEEL) and CELESC Distribuição S.A. for the financial support provided to the Research and Development Project No. 05697-0323/2023, entitled “Multifunctional Transportable Storage System Using First-Life and Second-Life Batteries for Outage Support and Seasonal Peak Demand Management in the Distribution Grid,” which is being developed under the ANEEL R&D Program, and to the Conselho Nacional de Desenvolvimento Científico e Tecnológico (CNPq – Project: 406361/2022-3) for the financial support. This research was also carried out within the scope of the activities of the National Institute for Technological Development of Photovoltaic Solar Energy Applications (INCT-DAESF, CNPq/MCTI/Brazil, Process 408486/2024-4).

6. References

Adebanjo, I. T., Eko, J., Agbeyegbe, A. G., Yuk, S. F., Cowart, S. V, Nagelli, E. A., Burpo, F. J., Allen, J. L., Tran, D. T., Bhattarai, N., Shah, K., Hwang, J.-Y., & Sun, H. H. (2025). A comprehensive review of lithium-ion battery components degradation and operational considerations: a safety perspective. Energy Adv., 4(7), 820–877. https://doi.org/10.1039/D5YA00065C.

Akram, M. N., & Abdul-Kader, W. (2024). Repurposing Second-Life EV Batteries to Advance Sustainable Development: A Comprehensive Review. In Batteries (Vol. 10, Issue 12). Multidisciplinary Digital Publishing Institute (MDPI). https://doi.org/10.3390/batteries10120452.

Antoniolli, A. F. ; M. A. A. ; R. R. (2017). Ônibus elétrico abastecido por edificação solar fotovoltaica. XIV ENCAC – Encontro Nacional Sobre Conforto No Ambiente Construído, 1472–1478.

Azizighalehsari, S., Venugopal, P., Pratap Singh, D., Batista Soeiro, T., & Rietveld, G. (2024). Empowering Electric Vehicles Batteries: A Comprehensive Look at the Application and Challenges of Second-Life Batteries. Batteries, 10(5). https://doi.org/10.3390/batteries10050161.

Beckers, C., Hoedemaekers, E., Dagkilic, A., & Bergveld, H. J. (2023). Round-Trip Energy Efficiency and Energy-Efficiency Fade Estimation for Battery Passport. 2023 IEEE Vehicle Power and Propulsion Conference (VPPC), 1–6. https://doi.org/10.1109/VPPC60535.2023.10403325.

Böttiger, M., Paulitschke, M., & Bocklisch, T. (2017). Systematic experimental pulse test investigation for parameter identification of an equivalent based lithium-ion battery model. Energy Procedia, 135, 337–346. https://doi.org/https://doi.org/10.1016/j.egypro.2017.09.525.

Cui, X., Aadil Khan, M., Singh, S., Sharma, R., & Onori, S. (2025). Toward a BMS2 Design Framework: Adaptive Data-Driven State-of-Health Estimation for Second-Life Batteries With BIBO Stability Guarantees. IEEE Transactions on Transportation Electrification, 11(3), 7684–7696. https://doi.org/10.1109/TTE.2025.3530498.

Edge, J., O'Kane, S., Prosser, R., Kirkaldy, N., Patel, A., Hales, A., Ghosh, A., Ai, W., Chen, J., Jiang, J., Li, S., Pang, M.-C., Bravo Diaz, L., Tomaszewska, A., Marzook, M., Radhakrishnan, K., Wang, H., Patel, Y., Wu, B., & Offer, G. (2021). Lithium-Ion Battery Degradation: What you need to know. Physical Chemistry Chemical Physics, 23. https://doi.org/10.1039/D1CP00359C.

Gharebaghi, M., Rezaei, O., Li, C., Wang, Z., & Tang, Y. (2025). A Survey on Using Second-Life Batteries in Stationary Energy Storage Applications. Energies, 18(1). https://doi.org/10.3390/en18010042.

Hohmann, M., Naspolini, H. F., Sergio, L. A. Z., Oliveira, A. K. V. de, Pacheco, L. F., & Rüther, R. (2024). AVALIAÇÃO DE MÉTODOS PARA CARACTERIZAÇÃO DE BATERIAS DE LÍTIO EM SEGUNDA VIDA. Anais Congresso Brasileiro de Energia Solar - CBENS. https://doi.org/10.59627/cbens.2024.2446.

Hong, H., Zhu, Y., & Shen, S. (2025). Evaluation of Lithium Battery Cycle Aging Based on Temperature Increase During Charging. https://doi.org/10.3390/batteries.

International Energy Agency. (2025). Global EV Outlook 2025 – Expanding sales in diverse markets. https://www.iea.org/reports/global-ev-outlook-2025.

Liu, L., Park, J., Lin, X., Sastry, A. M., & Lu, W. (2014). A thermal-electrochemical model that gives spatial-dependent growth of solid electrolyte interphase in a Li-ion battery. Journal of Power Sources, 268, 482–490. https://doi.org/https://doi.org/10.1016/j.jpowsour.2014.06.050.

O'Kane, S., Ai, W., Alonso-Albarez, D., Timms, R., Sulzer, V., Edge, J., Wu, B., Offer, G., & Marinescu, M. (2022). Lithium-ion battery degradation: how to model it. Physical Chemistry Chemical Physics, 24. https://doi.org/10.1039/D2CP00417H.

Oliveira, A., Gomes, A., Goulart, V., Montenegro, A., & Rüther, R. (2019). Analysis of the Integration of an Electric Bus and an Electric Vehicle with Grid-Connected PV Systems and a Storage System. 1–8. https://doi.org/10.18086/swc.2019.31.02.

Salek, F., Resalati, S., Babaie, M., Henshall, P., Morrey, D., & Yao, L. (2024). A Review of the Technical Challenges and Solutions in Maximising the Potential Use of Second Life Batteries from Electric Vehicles. Batteries, 10(3). https://doi.org/10.3390/batteries10030079.

Tao, T. S., Wei, G., & Zhang, X. (n.d.). PulseBat: A field-accessible dataset for second-life battery diagnostics from realistic histories using multidimensional rapid pulse test. https://doi.org/10.48550/arXiv.2502.16848.